ACS SENSORS

pubs.acs.org/acssensors

Article

Vertical Flow Cellulose-Based Assays for SARS-CoV-2 Antibody Detection in Human Serum

Seunghyeon Kim, Yining Hao, Eric A. Miller, Dousabel M. Y. Tay, Emma Yee, Patthara Kongsuphol, Huan Jia, Megan McBee, Peter R. Preiser, and Hadley D. Sikes*

Cite This: https://doi.org/10.1021/acssensors.1c00235

Read Online

ACCESS | Metrics & More | Article Recommendations | Supporting Information

ABSTRACT: Rapid and inexpensive serological tests for severe acute respiratory syndrome coronavirus-2 (SARS-CoV-2) antibodies are essential to conduct large-scale seroprevalence surveys and can potentially complement nucleic acid or antigen tests at the point of care. During the COVID-19 pandemic, extreme demand for traditional lateral flow tests has stressed manufacturing capacity and supply chains. Motivated by this limitation, we developed a SARS-CoV-2 antibody test using cellulose, an alternative membrane material, and a double-antigen sandwich format. Functionalized SARS-CoV-2 antigens were used as both capture and reporter binders, replacing the anti-human antibodies currently used in lateral flow tests. The test could provide enhanced sensitivity because it labels only antibodies against SARS-CoV-2 and the signal intensity is not diminished due to other human antibodies in serum. Three-dimensional channels in the assay were designed to have consistent flow rates and be easily manufactured by folding wax-printed paper. We demonstrated that this simple, vertical flow, cellulose-based assay could detect SARS-CoV-2 antibodies in clinical samples within 15 min, and the results were consistent with those from a laboratory, bead-based chemiluminescence immunoassay that was granted emergency use approval by the US FDA.

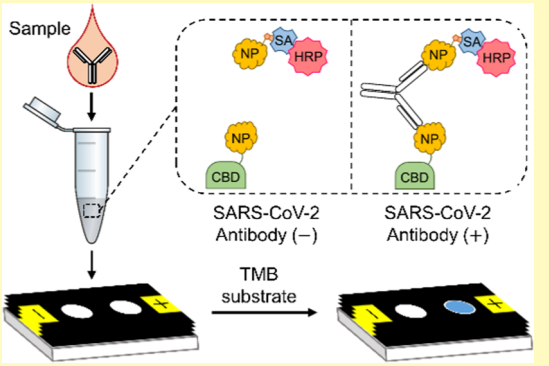

KEYWORDS: *SARS-CoV-2, COVID-19, serology, antibody, vertical flow, paper-based assay, cellulose-binding domain, horseradish peroxidase*

Serological testing for severe acute respiratory syndrome coronavirus-2 (SARS-CoV-2) antibodies has played a crucial role in monitoring and responding to COVID-19 pandemic. This kind of test detects antibodies produced in response to SARS-CoV-2 infection. Because antibodies persist in bodily fluids far longer than viral RNA or antigens, their presence provides information on both late-stage and past infections.[1] Therefore, serology has been used as a key tool in seroprevalence surveys to identify people who have been infected, but may not have been diagnosed due to mild illness or no symptoms, enabling a better understanding of transmission dynamics of the virus.[2] Furthermore, serology can assist nucleic acid or antigen tests to reduce false-negative results at a later stage of infection, where viral load is significantly reduced upon seroconversion.[3−7]

Enzyme-linked immunosorbent assays and magnetic bead-based chemiluminescent or fluorescent immunoassays are widely used for serological tests because these methods are relatively less expensive, high throughput, sensitive, and quantitative.[8−10] However, they may not be suitable for point-of-care testing or screening at massive scale, which is in high demand during the pandemic, because those methods depend on centralized-laboratory infrastructure and sample-transport logistics. Lateral flow assays, on the other hand, are rapid, easy-to-use, and instrument-free, providing qualitative results in 20 min.[1,10] Although their accuracy is not yet comparable to the lab-based methods,[9,11] this type of test may help conduct large-scale seroprevalence surveys and can potentially complement nucleic acid or antigen tests at the point of care if their manufacturing bottlenecks are resolved.

In most lateral flow assays authorized by the FDA under Emergency Use Authorization (EUA),[9] anti-human IgG and anti-human IgM antibodies are used as capture or reporter reagents in tests for SARS-CoV-2 antibodies. Used as capture reagents, anti-human IgG or IgM antibodies are deposited on separate test lines to capture IgG and IgM antibodies from patient samples. Used as reporter reagents, anti-human antibodies conjugated to nanoparticles are used to label SARS-CoV-2-specific antibodies captured from patient samples

Received: February 3, 2021
Accepted: March 25, 2021

Scheme 1. Vertical-Flow Paper-Based Assays for SARS-CoV-2 Antibody Detection[a]

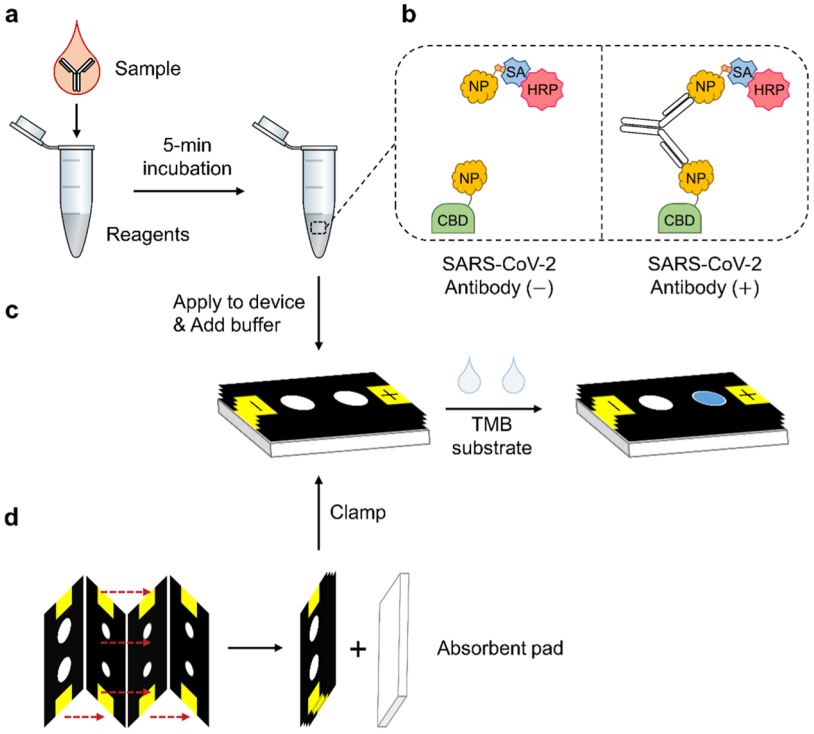

[a](a) Human serum is incubated with reagents including SARS-CoV-2 nucleocapsid protein fused to cellulose-binding domain (NP-CBD), biotinylated NP (NP-biotin), and streptavidin horseradish peroxidase conjugate (SA-HRP). (b) The NP−enzyme complex (NP-biotin-SA-HRP) is coupled with NP-CBD only in the presence of target antibodies. (c) The mixture of sample and reagents is applied to a cellulose-based test zone, immediately followed by washing buffer and then TMB substrate solution. The positive test zone produces blue color because antibodies against SARS-CoV-2 immobilize HRP on the test zone through the interaction between NP-CBD and cellulose. (d) The paper-based assays are prepared by folding wax-printed four-layer paper devices and clamping them to absorbent pads.

by SARS-CoV-2 antigens deposited on test lines. However, these strategies intrinsically reduce the sensitivity of assays because other human IgG (7−16 g/L) and IgM (0.4−2.3 g/L) antibodies are commonly present in blood[12] regardless of SARS-CoV-2 infection and they compete with target SARS-CoV-2 antibodies, if present, for binding with the anti-human antibody reagents. A double-antigen sandwich format,[13,14] on the other hand, leverages the multivalency of target antibodies (IgG and IgM) using functionalized antigens as both capture and reporter reagents, replacing the anti-human antibodies. This design can potentially improve assay sensitivity because it prevents diminished signals due to non-SARS-CoV-2 antibodies in blood.[13−15]

To assess this double-antigen strategy, we created a vertical flow, cellulose-based SARS-CoV-2 antibody assay with two motivations. First, this platform can provide an alternative to traditional lateral flow assays. This cellulose-based assay uses orthogonal materials (e.g., cellulose and enzymes) to those (e.g., nitrocellulose membrane, nanoparticles, and anti-human antibodies) required for lateral flow assays. The vertical flow channel can be manufactured by folding wax-printed paper[16,17] versus aligning many different pads and sealing with cassettes or adhesives to make lateral flow assays.[18] Second, we wanted to explore using a cellulose-binding domain (CBD) as a fusion partner for an antigen, which we hypothesized would allow rapid immobilization of SARS-CoV-2 antigens with oriented display on a cellulosic test zone via specific interactions between CBD and cellulose. As described in earlier work on the topic of antigen[19] rather than serology tests, this CBD fusion method can yield approximately 90% immobilization efficiency with only 30 s of contact, suggesting promise for quick and sensitive serological tests.

We chose SARS-CoV-2 nucleocapsid protein (NP) as the antigen for the target antibodies because NP was the most abundant antigen at the early stage of SARS-CoV infection and initiated a strong antibody response.[20−22] A new study supports this idea that detection of antibodies against SARS-CoV-2 NP is more sensitive than antibodies against the other commonly used antigen, spike protein.[23] In the present study, we probed importance of the flow rate in the assay and optimized production of NP and NP-CBD in bacterial hosts. Using NP-CBD as the capture reagent and biotinylated NP (NP-biotin) with streptavidin horseradish peroxidase conjugate (SA-HRP) as the reporter reagent, we successfully demonstrated that target antibodies simultaneously associated with both NP-CBD and NP-biotin-SA-HRP were immobilized on the cellulosic test zone. Finally, we verified the function of the vertical flow assay with inactivated clinical samples, confirming that sera from SARS-CoV-2 infected patients produced distinctively higher colorimetric signals than sera from healthy individuals.

RESULTS AND DISCUSSION

To prevent the interference of other human antibodies in serological tests and achieve more sensitive detection of SARS-CoV-2 antibodies, we adopted a double-antigen sandwich format[13,14] in a vertical flow paper-based assay (Scheme 1). In this test, SARS-CoV-2 nucleocapsid protein (NP) is used as an

https://doi.org/10.1021/acssensors.1c00235
ACS Sens. XXXX, XXX, XXX−XXX

affinity tag for target antibodies in both capture and reporter reagents, using the multivalency of antibodies. Unlike other tests using anti-human antibodies, this approach cannot distinguish between SARS-CoV-2 IgG and IgM antibodies. However, given the range of temporal IgG and IgM expression observed across patients,[6,7,24] the ability to detect both antibodies expands the flexibility of this test and concentrates signal in one location for potentially augmented sensitivity. The capture and reporter reagents used in this assay are NP fused to cellulose-binding domain (CBD) and biotinylated NP (NP-biotin), respectively. The biotin on NP serves to conjugate NP with horseradish peroxidase (HRP) via strong biotin−streptavidin (SA) interaction. Thus, when a patient sample is mixed with the reagents, the reporting enzyme (HRP) will be associated with CBD to form enzyme-antibody-CBD sandwich complexes as patient antibodies link the capture and reporter reagents (Scheme 1a,b). Following the incubation, the sample-reagent mixture is applied to cellulose test zone, where the enzyme-antibody-CBD complexes are immobilized through specific binding between CBD and cellulose (Scheme 1c). Aided by addition of wash buffer, other complexes without CBD flow through the vertical channel and arrive at the absorbent pad. Upon addition of a 3,3′,5,5′-tetramethylbenzidine (TMB) substrate solution containing a stable peroxide (Thermo Fisher 34028), test zones with blue color indicate positive patient samples. Notably, because the color develops on the top layer, unfolding the device is not required to interpret the results. As illustrated in Scheme 1d, we designed the vertical flow channel to have four layers with a large circular region on the top layer and a smaller circular region on the following layers as this channel could achieve more consistent flow rates than a single-layer device (Figure 1), and also slower flow rates, promoting reliably high

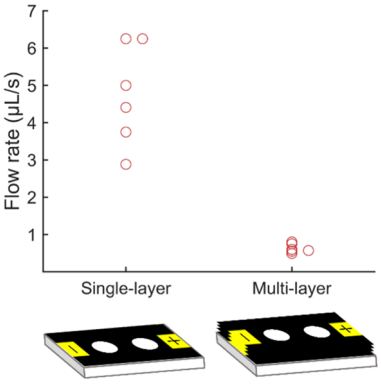

Figure 1. Comparison of flow rates in single-layer devices and multilayer (four-layer) devices. Single-layer and multilayer (four-layer) vertical flow test strips were clamped together with absorbent pads. To each device, 50 μL of human serum and 25 μL of washing buffer (1 × PBS) were added. The time required to absorb all solutions was measured to calculate average flow rates. Six replicates were conducted for both single-layer and multilayer devices. Raw data are available in Table S1.

CBD capture efficiency. In this study, the three-dimensional channel was fabricated using wax-printed paper folded manually. However, the design is amenable to large-scale manufacturing using an industrial paper-folding machine.

In designing our capture reagent, we cloned NP with CBD on the C-terminus (NP-CBD) and N-terminus (CBD-NP) to compare their performance. The two variants were expressed in BL21 (DE3) *Escherichia coli* and purified with IMAC resin. NP-CBD was successfully purified, and its purity was checked by SDS-PAGE (Figure 2A). However, after purification of

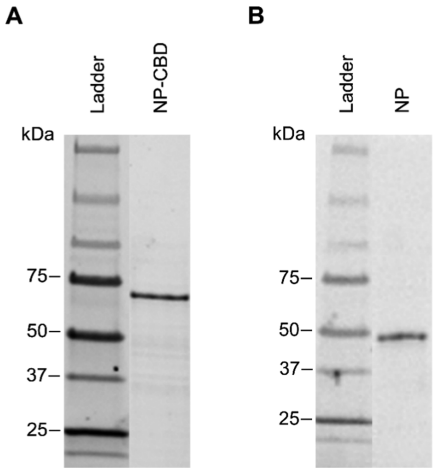

Figure 2. SDS-PAGE gel image of purified recombinant products. (A) NP-CBD band is observed near its theoretical molecular weight (66 kDa). (B) NP band is observed at approximately 48 kDa. The full gel images are available in Figure S1.

CBD-NP, truncated products with lower molecular weight were observed (Figure S2). Despite the addition of various amounts of protease inhibitor during the cell lysing process, it was not possible to significantly reduce these truncation products. It is likely that the translation of N-terminus CBD-NP was terminated prematurely *in vivo*. Therefore, NP-CBD was chosen to be the capture reagent for the remainder of this study.

To generate biotinylated NP as the reporter molecule, we attempted to biotinylate the NP *in vivo*. A biotin acceptor peptide, AviTag, that enables *in vivo* enzymatic biotinlyation during protein expression was fused to the N-terminus of NP. To improve the accessibility of the biotin acceptor peptide, a flexible $(G_4S)_2$ linker sequence was inserted between the AviTag and NP sequence. After purification, NP was avidin purified to exclude any nonbiotinylated portion of NP. The extent of *in vivo* biotinylation was very low, making it impossible to quantify by the bicinchoninic acid assay. One possible reason was that the linker was insufficient to facilitate the access of biotin. We therefore sought to biotinylate the recombinant NP through a chemical method. The purified NP (Figure 2B) was reacted with an *N*-hydroxysuccinimide ester derivative of biotin. The labeling efficiency was 1.3 biotin per NP.

We then investigated the effect of reagent concentrations on the assay performance (Figure 3). Here, negative and positive control samples were prepared by spiking 0 and 40 nM SARS-CoV-2 NP monoclonal rabbit antibody into human serum to simulate nonspecific binding signals (N) and specific binding signals (S). In the first experiment, we varied the concentration of SA-HRP in the reagent mixture with fixed concentrations of NP-CBD and NP-biotin (Figure 3A). The blue color intensity increased in both 0 and 40 nM antibody-spiked samples as higher concentrations of SA-HRP were used. The increasing trend of signal difference ($S-N$) indicates that, at higher concentrations of the enzyme, more SA-HRP actually labeled (NP-CBD)-(antibody)-(NP-biotin) complexes rather than

https://doi.org/10.1021/acssensors.1c00235
ACS Sens. XXXX, XXX, XXX−XXX

A

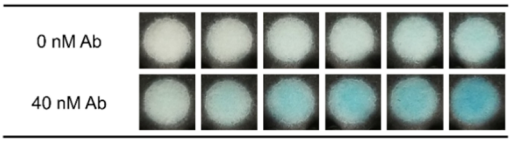

[SA-HRP] (pM)	0 nM Ab (N)	40 nM Ab (S)	S/N	S-N	S/N×(S-N)
100	0.010	0.068	6.800	0.058	0.394
200	0.030	0.134	4.467	0.104	0.465
300	0.056	0.235	4.196	0.179	0.751
400	0.071	0.292	4.113	0.221	0.909
500	0.107	0.306	2.860	0.199	0.569
750	0.156	0.444	2.846	0.288	0.820

B

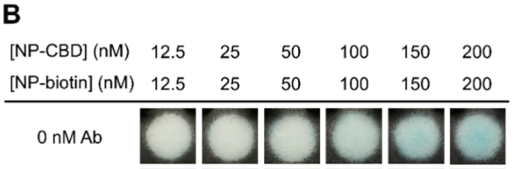

[NP-CBD], [NP-biotin] (nM)	0 nM Ab (N)	40 nM Ab (S)	S/N	S-N	S/N×(S-N)
12.5	0.022	0.077	3.500	0.055	0.193
25	0.020	0.075	3.750	0.055	0.206
50	0.041	0.152	3.707	0.111	0.412
100	0.087	0.243	2.793	0.156	0.436
150	0.132	0.246	1.864	0.114	0.212
200	0.176	0.274	1.557	0.098	0.153

Figure 3. Effect of reagent concentrations in the sample−reagent mixture on the assay performance. (A) The concentration of SA-HRP was varied while each concentration of NP-CBD and NP-biotin was fixed at 100 nM. (B) The concentrations of NP-CBD and NP-biotin were varied with the concentration of SA-HRP fixed at 400 pM, the optimal value from the previous experiment. Under each condition, positive controls were prepared by spiking 40 nM SARS-CoV-2 NP antibody (40 nM Ab) into human serum, and negative controls were human serum without the antibody (0 nM Ab). The signal from each test zone was obtained by quantifying the cyan intensity of its color. The ratio of specific binding signals (S) to nonspecific binding signals (N) and their difference ($S-N$) were chosen to evaluate the assay performance under each condition.

being nonspecifically bound to the test zone. Next, we explored different concentrations of NP-CBD and NP-biotin with fixed concentration of SA-HRP (Figure 3B). Kinetic modeling of the binding reactions (Figure 4) indicated that equimolar amounts of NP-CBD and NP-biotin would maximize the number of antibody complexes labeled with both NP-CBD and NP-biotin, and for this reason, we maintained an equimolar concentration of the capture (NP-CBD) and reporter (NP-biotin) proteins throughout the optimization. The blue color intensity increased in both 0 and 40 nM antibody-spiked samples as higher concentrations of NP-CBD and NP-biotin were used. However, a maximal signal difference ($S-N$) was obtained when 100 nM of NP-CBD and NP-biotin were used with higher concentrations, leading to a decrease of $S-N$. The data suggests that while more antibodies can be labeled with both CBD and HRP when higher concentrations of NP-CBD and NP-biotin are used, it also contributes to nonspecific binding of SA-HRP to cellulose paper. We speculate that more NP-biotin is nonspecifically bound to paper when used at a

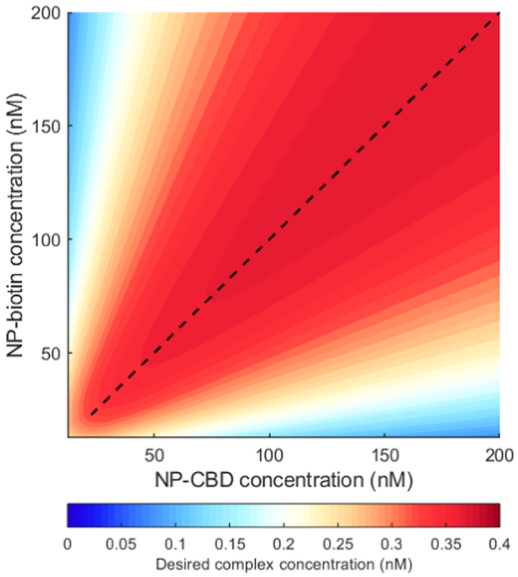

Figure 4. Formation of desired antibody complex from various concentrations of NP-CBD and NP-biotin. The concentration of the desired complex is presented as a heat map. The dotted line indicates that an equimolar concentration of NP-CBD and NP-biotin can produce the highest concentration of the desired complex. The model simulated the binding kinetics within NP-CBD, NP-biotin, and 1 nM patient antibody mixture for 15 min. Detailed information on the kinetic modeling is available in Figure S3.

higher concentration, causing more SA-HRP to immobilize on paper even without SARS-CoV-2 NP antibodies.

To achieve a low limit of detection as well as high sensitivity, it is essential to reduce nonspecific binding signals (N) and enhance specific binding signals (S). Thus, we compared the signal ratio (S/N) and the signal difference ($S-N$) under each condition (Figure 3). Notably, neither higher S/N values nor higher $S-N$ values could help find the best condition that provided both the smallest N and the largest S because none of them alone could reflect the whole picture. The largest S/N value was obtained with the smallest N at 100 pM SA-HRP (Figure 3A) even though the S value was relatively small. The largest $S-N$ value resulted from the largest S at 750 pM SA-HRP (Figure 3A), but the N value was also too high. Therefore, we chose $S/N \times (S-N)$ as an objective function to optimize N and S at the same time and maximized it at 400 pM SA-HRP, 100 nM NP-CBD, and 100 nM NP-biotin.

After optimizing the reagent concentrations, we assessed the sensitivity of the vertical flow SARS-CoV-2 antibody test using SARS-CoV-2 NP rabbit antibody as a mock target, spiked into human serum. As demonstrated in Figure 5A, higher concentrations of the antibody produced more intense blue color. We quantified the color intensity of each image in the cyan channel and defined the LOD by requiring signals greater than the mean intensity of the 0 nM samples plus three standard deviations above the mean, resulting in an LOD of 5 nM (Figure 5B). At this LOD concentration, the lowest cyan intensity was 0.186, so we defined it as a cutoff value for distinguishing between positive and negative samples.

Finally, we tested three clinical samples in both vertical flow paper-based assays and magnetic bead-based chemiluminescence immunoassays (Figure 6). Biosafety standards at the time required inactivation of clinical samples with 1 v/v% Triton X-100, so negative control samples were also prepared

https://doi.org/10.1021/acssensors.1c00235
ACS Sens. XXXX, XXX, XXX−XXX

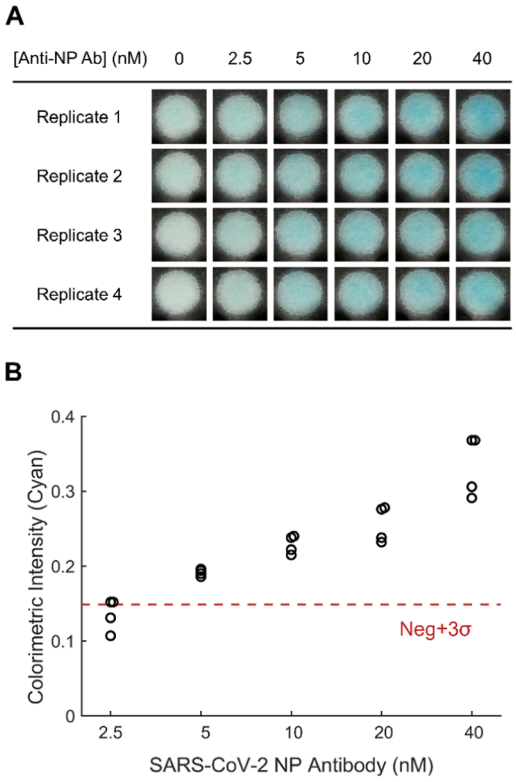

Figure 5. Dose response curve for the vertical flow paper-based assays with SARS-CoV-2 NP antibody spiked into human serum. (A) Images of the assay results. Four replicates were obtained at each concentration of the antibody. (B) Colorimetric intensity (cyan) values were calculated using ImageJ. The Neg + 3σ line was determined with the mean cyan intensity (Neg) of 0 nM samples and their standard deviation (σ), demonstrating that the limit of detection for the antibody is around 5 nM.

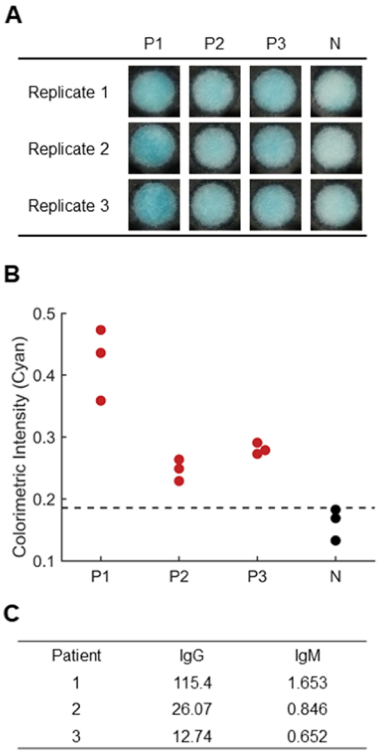

C

Patient	IgG	IgM
1	115.4	1.653
2	26.07	0.846
3	12.74	0.652

Figure 6. Clinical sample analysis comparing the vertical-flow paper-based assay and magnetic bead-based chemiluminescence immunoassay. (A) Images of the assay results with three PCR-confirmed SARS-CoV-2 patient samples (P1, P2, and P3) and human serum collected before the SARS-CoV-2 pandemic. (B) Colorimetric intensity (cyan) values were calculated using ImageJ. All patient samples show higher colorimetric intensity than the cutoff represented as a dotted line. Negative sample data lie below the cutoff. (C) Magnetic bead-based chemiluminescence immunoassay[25] results show the IgG and IgM levels in the patient samples (arbitrary units).

by treating human serum with 1 v/v% Triton X-100.[26] All three SARS-CoV-2 patient samples with three replicates produced stronger blue color than negative samples, which can be differentiated by the naked eye (Figure 6A). A color chart or, better yet, a colorimetric reader with automated image analysis would be useful for unambiguous interpretation of test results. Quantitative colorimetric intensities from all three patient samples were notably higher than the predetermined cutoff value, whereas the negative control samples produced lower colorimetric intensity than the cutoff (Figure 6B). Comparing Figure 6B with Figure 5B, the signals from negative samples increased slightly due to the addition of Triton X-100. The assay results agreed with the chemiluminescence immunoassay results obtained using Diazyme DZ-Lite SARS-CoV-2 IgG and IgM CLIA Kits (Figure 6C). These assays have been authorized by FDA under an EUA for use by authorized laboratories.[27] Clinical sensitivity for SARS-CoV-2 IgG detection is 96.2% positive percent agreement (PPA) against RT-PCR after >7 days post symptom onset and 100% PPA after ≥15 days post symptom onset.[27] Clinical sensitivity for SARS-CoV-2 IgM detection is 92.1% PPA after >7 days post symptom onset and 93.9% PPA after ≥15 days post symptom onset.[27] With the paper-based assays, we expected that a much higher concentration of antibodies was included in patient sample 1 (P1), which was confirmed by the chemiluminescence immunoassay. However, there was slight inconsistency in patient sample 2 (P2) and patient sample 3 (P3). According to the chemiluminescence assay results, the signals from SARS-CoV-2 antibodies were higher in P2 than in P3, but the trend was opposite in the paper-based assays. We speculate that the difference could result from what antigens were used to detect SARS-CoV-2 antibodies. In our design, we used only SARS-CoV-2 NP, but the chemiluminescence assay used both the NP and spike protein. It is possible that more spike protein-specific antibodies were present in P2 than in P3. In addition, we assessed the performance of vertical flow paper-based assays with immobilized NP-CBD that used HRP-conjugated anti-human IgG or anti-human IgM antibodies as reporter reagents (Figure S4). Unsurprisingly, the signal intensity from antibody-positive samples was much lower than in the double-antigen format presumably due to interfering non-SARS-CoV-2 IgG and IgM antibodies.

A much larger number of clinical samples must be analyzed using the vertical flow cellulose-based tests reported herein to calculate clinical sensitivity, specificity, and PPA values. Institutional biosafety policies precluded such a study. However, the finding that patient antibodies in a small number of inactivated SARS-CoV-2 positive samples recognized both the NP-CBD and biotinylated NP reagents we developed, and that results using the new cellulose-based assay agreed with results from a laboratory-based test that has been granted EUA by the FDA motivated a follow-up study that will be reported separately with clinical collaborators.

https://doi.org/10.1021/acssensors.1c00235
ACS Sens. XXXX, XXX, XXX−XXX

CONCLUSIONS

We demonstrated that vertical-flow, cellulose-based tests can successfully detect SARS-CoV-2 antibodies in human serum using functionalized SARS-CoV-2 nucleocapsid protein as both capture and reporter reagents. By replacing anti-human antibodies as capture or reporter reagents, we could reduce the interference from non-SARS-CoV-2 human antibodies. In addition, specific interaction between cellulose and cellulose-binding domain (CBD) of the capture reagent allowed the cellulose-based test zone to rapidly and selectively immobilize reporting enzyme (HRP) associated with CBD in the presence of target antibodies. More detailed studies of the reaction and transport rates in this new system are warranted, with a variety of grades of cellulose in addition to the one used here, offering further control of flow rates and reaction rates between CBD and cellulose that can be used to tune analytical performance. This work reveals the possibility of using cellulose-based assays for extensive serological testing. We hope that this simple, rapid, and easy-to-scale approach to serological testing can be implemented to help large-scale SARS-CoV-2 seroprevalence surveys and complement other SARS-CoV-2 diagnostic tests at the point of care.

MATERIALS AND METHODS

Materials. Human serum (H4522), 10 × phosphate-buffered saline (PBS), D-biotin (B4639), and Microspin G-25 columns (GE27-5325-01) were purchased from Millipore Sigma (St. Louis, MO). Streptavidin horseradish peroxidase conjugate (SA-HRP) (N100), TMB substrate solution (34028), 10% BSA in 1 × PBS (37525), Pierce BCA Protein Assay Kit (23225), Pierce Monomeric Avidin Agarose Kit (432040), EZ-Link Sulfo-NHS-LC-Biotin (A39257), and Halt protease inhibitor cocktail (100×) (87786) were purchased from Thermo Fisher Scientific (Waltham, MA). SARS-CoV-2 NP antibody (40143-R019) was purchased from Sino Biological (Wayne, PA). Whatman Grade 1 Chr Cellulose Chromatography paper (21427-003), glycerol (97062-452), Kanamycin sulfate (97061-600), Terrific Broth Powder (97063-418), and isopropyl-β-D-thiogalactoside (IPTG) 99% dioxane-free (AAB21149-06) were obtained from VWR (Radnor, PA). Blot paper (1703965), 4−15% Mini-PROTEAN TGX Stain-Free Precast Gels (4568083), Precision Plus Protein All Blue Prestained Protein Standards (1610373), Precision Plus Protein Unstained Standards (1610363), and Nuvia IMAC Resin (7800800) were purchased from Bio-Rad Laboratories, Inc. (Hercules, CA). Restriction enzyme *Nde*I (R0111S), *Xho*I (R0146S), *Bam*HI (R3136S), and *Eco*RI (R3101S) were purchased from New England BioLabs (Ipswich, MA). Human serum samples collected from PCR-confirmed SARS-CoV-2-positive patients were purchased from Brio Systems and Curebase. These biobanked samples were collected with informed consent and IRB approval (IntegReview, CURE19-001) and provided deidentified.

Production of Gene Constructs. Recombinant SARS-CoV-2 nucleocapsid protein (NP) was cloned into the pET28b(+) between *Nde*I and *Xho*I restriction sites for bacteria expression. The NP sequence was acquired from NCBI[28] and synthesized by Genewiz. To make NP with cellulose-binding domain (CBD) on the C-terminus, the NP sequence was amplified by *NP-CBD-For* and *C19 NR* primers at an annealing temperature of 58.9 °C. *Nde*I and *Bam*HI restriction sites were appended to the appropriate end of the sequence. The amplicon was then subjected to the double digestion with *Nde*I and *Bam*HI restriction enzymes at 37 °C for an hour. The insert was then ligated into double digested backbone vector pET28b(+) rcSso7d.SA-CBD as previously described.[29]

To make NP with CBD on the N-terminus, the type 3a CBD was amplified by *N-CBD-for* and *N-term-CBD-Linker-rev* primers using previously described rcSso7d.SA-CBD as a template.[28] A $(G_4S)_3$ linker as well as a *Bam*HI restriction site were appended to the CBD sequence in this PCR reaction. The NP sequence was amplified by *C-term-NP-for* and *C-term-NP-rev* primers, appending *Bam*HI and *Xho*I restriction sites. The products of the two PCR reactions were subjected to restriction digest by *Bam*HI and the digested products were ligated together. The ligated product was subjected to the double digestion by *Nde*I and *Xho*I and was then ligated into double digested backbone pET28b(+) rcSso7d.SA-CBD.[29]

A construct of NP with N-terminus AviTag[30] (BA-NP) was generated to allow *in vivo* biotinylation of NP. The NP sequence was amplified by *EcoRI-Covid19NP-Forward* and *Covid19NP-XhoI-Rev* primers at an annealing temperature of 55.2 °C. The amplicon was double digested by *Eco*RI and *Xho*I at 37 °C for an hour and ligated into digested pET28b(+) N terminal BA-MBP-rcSso7d vector previously described.[31]

Forward and reverse primers were designed and characterized using the IDT Oligoanalyzer tool, and the oligonucleotide sequences are reported in Table S2. Protein sequences are provided in Table S3.

Protein Expression, Purification, and Characterization. Details are provided in the Supporting Information.

Vertical-Flow Paper-Based Assays. Test strips were made by wax-printing four layers containing wax-free circular regions on Whatman Grade 1 cellulose paper and melting the wax-printed paper in an oven at 150 °C for 30 s. The final diameter of hydrophilic wells in the top layer and in the following layers were 3 and 2.5 mm, respectively. The wax-free surface was blocked with 5% BSA in 1 × PBS. The four-layer devices were then folded and clamped together with absorbent pad (blot paper). Standard reagent solution was prepared by mixing two parts of 1.6 nM SA-HRP, one part of 800 nM NP-CBD, and one part of 800 nM NP-biotin to give 800 pM SA-HRP, 200 nM NP-CBD, and 200 nM NP-biotin in 1% BSA in 1 × PBS. For one test, 25 μL of human serum was mixed with the same volume of the reagent solution and incubated for 5 min. This sample−reagent mixture (50 μL) was applied to test zone. Following the sample loading, the test zone was washed with 1 × PBS (25 μL). Finally, 10 μL of TMB substrate solution was added to the test zone and imaged after 5 min.

Colorimetric Analysis. Test zone images were opened in ImageJ, and the circular region was selected and converted from RGB to CMYK. The selected image was separated into cyan, magenta, yellow, and black channels. The colorimetric intensity in the cyan channel was measured and used for further analysis.

Inactivation of Clinical Samples. Human serum samples collected from PCR-confirmed positive patients were treated with 1% Triton X-100 for 30 min according to the inactivation protocol[26] and stored at −20 °C before use.

ASSOCIATED CONTENT

Supporting Information

The Supporting Information is available free of charge at https://pubs.acs.org/doi/10.1021/acssensors.1c00235.

Methods: protein expression, purification, and characterization; chemical biotinylation of NP and characterization; raw data for calculating flow rates in single-layer and multilayer devices (Table S1); oligonucleotide sequences of primers (Table S2); protein sequences (Table S3); original SDS-PAGE gel images of purified reagent proteins (Figure S1); comparison of SDS-PAGE gel images of NP-CBD and CBD-NP (Figure S2); formation of desired antibody complex (CBD-NP-Ab-NP-biotin) from various concentrations of NP-CBD and NP-biotin (Figure S3); analysis of clinical samples with vertical-flow antigen-down immunoassays and enzyme-linked immunosorbent assays (Figure S4) (PDF)

https://doi.org/10.1021/acssensors.1c00235
ACS Sens. XXXX, XXX, XXX−XXX

AUTHOR INFORMATION

Corresponding Author

Hadley D. Sikes − *Department of Chemical Engineering, Massachusetts Institute of Technology, Cambridge, Massachusetts 02139, United States; Program in Polymers and Soft Matter, Massachusetts Institute of Technology, Cambridge, Massachusetts 02139, United States; Antimicrobial Resistance Interdisciplinary Research Group, Singapore-MIT Alliance for Research and Technology, Singapore 138602;* orcid.org/0000-0002-7096-138X; Email: sikes@mit.edu

Authors

Seunghyeon Kim − *Department of Chemical Engineering, Massachusetts Institute of Technology, Cambridge, Massachusetts 02139, United States;* orcid.org/0000-0001-6515-2679

Yining Hao − *Department of Chemical Engineering, Massachusetts Institute of Technology, Cambridge, Massachusetts 02139, United States*

Eric A. Miller − *Department of Chemical Engineering, Massachusetts Institute of Technology, Cambridge, Massachusetts 02139, United States*

Dousabel M. Y. Tay − *Department of Chemical Engineering, Massachusetts Institute of Technology, Cambridge, Massachusetts 02139, United States*

Emma Yee − *Department of Chemical Engineering, Massachusetts Institute of Technology, Cambridge, Massachusetts 02139, United States*

Patthara Kongsuphol − *Antimicrobial Resistance Interdisciplinary Research Group, Singapore-MIT Alliance for Research and Technology, Singapore 138602*

Huan Jia − *Antimicrobial Resistance Interdisciplinary Research Group, Singapore-MIT Alliance for Research and Technology, Singapore 138602*

Megan McBee − *Antimicrobial Resistance Interdisciplinary Research Group, Singapore-MIT Alliance for Research and Technology, Singapore 138602*

Peter R. Preiser − *Antimicrobial Resistance Interdisciplinary Research Group, Singapore-MIT Alliance for Research and Technology, Singapore 138602; School of Biological Sciences, Nanyang Technological University Singapore, Singapore 639798, Singapore*

Complete contact information is available at: https://pubs.acs.org/10.1021/acssensors.1c00235

Author Contributions

The paper was written through contributions of all authors.

Funding

The Deshpande Center for Technological Innovation and MIT alumni and family donors supported the work at MIT. The Singapore Ministry of Health's National Medical Research Council supported the work at SMART and NTU under its COVID-19 Research Fund (COVID19RF2-0044).

Notes

The authors declare no competing financial interest.

ACKNOWLEDGMENTS

The authors thank Brio Systems and Curebase for making well-characterized and deidentified clinical samples commercially available, and LabShares of Newton, MA, for hosting experiments with clinical samples that were not possible at MIT.

REFERENCES

(1) Kilic, T.; Weissleder, R.; Lee, H. Molecular and Immunological Diagnostic Tests of COVID-19: Current Status and Challenges. *iScience* **2020**, *23*, No. 101406.

(2) Havers, F. P.; Reed, C.; Lim, T.; Montgomery, J. M.; Klena, J. D.; Hall, A. J.; Fry, A. M.; Cannon, D. L.; Chiang, C. F.; Gibbons, A.; Krapiunaya, I.; Morales-Betoulle, M.; Roguski, K.; Rasheed, M. A. U.; Freeman, B.; Lester, S.; Mills, L.; Carroll, D. S.; Owen, S. M.; Johnson, J. A.; Semenova, V.; Blackmore, C.; Blog, D.; Chai, S. J.; Dunn, A.; Hand, J.; Jain, S.; Lindquist, S.; Lynfield, R.; Pritchard, S.; Sokol, T.; Sosa, L.; Turabelidze, G.; Watkins, S. M.; Wiesman, J.; Williams, R. W.; Yendell, S.; Schiffer, J.; Thornburg, N. J. Seroprevalence of Antibodies to SARS-CoV-2 in 10 Sites in the United States, March 23-May 12, 2020. *JAMA Intern. Med.* **2020**, *30329*, 1−11.

(3) Marca, A.; La; Capuzzo, M.; Paglia, T.; Roli, L.; Trenti, T.; Nelson, S. M. Testing for SARS-CoV-2 (COVID-19): A Systematic Review and Clinical Guide to Molecular and Serological in-Vitro Diagnostic Assays. *Reprod. Biomed. Online* **2020**, *41*, 483−499.

(4) To, K. K.-W.; Tsang, O. T.-Y.; Leung, W.-S.; Tam, A. R.; Wu, T.-C.; Lung, D. C.; Yip, C. C.-Y.; Cai, J.-P.; Chan, J. M.-C.; Chik, T. S.-H.; Lau, D. P.-L.; Choi, C. Y.-C.; Chen, L.-L.; Chan, W.-M.; Chan, K.-H.; Ip, J. D.; Ng, A. C.-K.; Poon, R. W.-S.; Luo, C.-T.; Cheng, V. C.-C.; Chan, J. F.-W.; Hung, I. F.-N.; Chen, Z.; Chen, H.; Yuen, K.-Y. Temporal Profiles of Viral Load in Posterior Oropharyngeal Saliva Samples and Serum Antibody Responses during Infection by SARS-CoV-2: An Observational Cohort Study. *Lancet Infect. Dis.* **2020**, *20*, 565−574.

(5) Zhao, J.; Yuan, Q.; Wang, H.; Liu, W.; Liao, X.; Su, Y.; Wang, X.; Yuan, J.; Li, T.; Li, J.; Qian, S.; Hong, C.; Wang, F.; Liu, Y.; Wang, Z.; He, Q.; Li, Z.; He, B.; Zhang, T.; Fu, Y.; Ge, S.; Liu, L.; Zhang, J.; Xia, N.; Zhang, Z. Antibody Responses to SARS-CoV-2 in Patients of Novel Coronavirus Disease 2019. *Clin. Infect. Dis.* **2020**, No. ciaa344.

(6) Lee, C. Y.-P.; Lin, R. T. P.; Renia, L.; Ng, L. F. P. Serological Approaches for COVID-19: Epidemiologic Perspective on Surveillance and Control. *Front. Immunol.* **2020**, *11*, 1−7.

(7) Long, Q.-X.; Liu, B.-Z.; Deng, H.-J.; Wu, G.-C.; Deng, K.; Chen, Y.-K.; Liao, P.; Qiu, J.-F.; Lin, Y.; Cai, X.-F.; Wang, D.-Q.; Hu, Y.; Ren, J.-H.; Tang, N.; Xu, Y.-Y.; Yu, L.-H.; Mo, Z.; Gong, F.; Zhang, X.-L.; Tian, W.-G.; Hu, L.; Zhang, X.-X.; Xiang, J.-L.; Du, H.-X.; Liu, H.-W.; Lang, C.-H.; Luo, X.-H.; Wu, S.-B.; Cui, X.-P.; Zhou, Z.; Zhu, M.-M.; Wang, J.; Xue, C.-J.; Li, X.-F.; Wang, L.; Li, Z.-J.; Wang, K.; Niu, C.-C.; Yang, Q.-J.; Tang, X.-J.; Zhang, Y.; Liu, X.-M.; Li, J.-J.; Zhang, D.-C.; Zhang, F.; Liu, P.; Yuan, J.; Li, Q.; Hu, J.-L.; Chen, J.; Huang, A.-L. Antibody Responses to SARS-CoV-2 in Patients with COVID-19. *Nat. Med.* **2020**, *26*, 845−848.

(8) https://www.centerforhealthsecurity.org/resources/COVID-19/serology/Serology-based-tests-for-COVID-19.html (Accessed on Sept 30, 2020).

(9) https://www.fda.gov/medical-devices/coronavirus-disease-2019-covid-19-emergency-use-authorizations-medical-devices/eua-authorized-serology-test-performance (Accessed on Sept 30, 2020).

(10) Ravi, N.; Cortade, D. L.; Ng, E.; Wang, S. X. Diagnostics for SARS-CoV-2 Detection: A Comprehensive Review of the FDA-EUA COVID-19 Testing Landscape. *Biosens. Bioelectron.* **2020**, *165*, No. 112454.

(11) Whitman, J. D.; Hiatt, J.; Mowery, C. T.; Shy, B. R.; Yu, R.; Yamamoto, T. N.; Rathore, U.; Goldgof, G. M.; Whitty, C.; Woo, J. M.; Gallman, A. E.; Miller, T. E.; Levine, A. G.; Nguyen, D. N.; Bapat, S. P.; Balcerek, J.; Bylsma, S. A.; Lyons, A. M.; Li, S.; Wong, A. W.; Gillis-Buck, E. M.; Steinhart, Z. B.; Lee, Y.; Apathy, R.; Lipke, M. J.; Smith, J. A.; Zheng, T.; Boothby, I. C.; Isaza, E.; Chan, J.; Acenas, D. D., II; Lee, J.; Macrae, T. A.; Kyaw, T. S.; Wu, D.; Ng, D. L.; Gu, W.; York, V. A.; Eskandarian, H. A.; Callaway, P. C.; Warrier, L.; Moreno, M. E.; Levan, J.; Torres, L.; Farrington, L. A.; Loudermilk, R.; Koshal, K.; Zorn, K. C.; Garcia-Beltran, W. F.; Yang, D.; Astudillo, M. G.; Bernstein, B. E.; Gelfand, J. A.; Ryan, E. T.; Charles, R. C.; Iafrate, A.

J.; Lennerz, J. K.; Miller, S.; Chiu, C. Y.; Stramer, S. L.; Wilson, M. R.; Manglik, A.; Ye, C. J.; Krogan, N. J.; Anderson, M. S.; Cyster, J. G.; Ernst, J. D.; Wu, A. H. B.; Lynch, K. L.; Bern, C.; Hsu, P. D.; Marson, A. Test Performance Evaluation of SARS-CoV-2 Serological Assays. *medRiv Preprint* **2020**, DOI: 10.1101/2020.04.25.20074856.

(12) Dati, F.; Schumann, G.; Thomas, L.; Aguzzi, F.; Baudner, S.; Bienvenu, J.; Blaabjerg, O.; Blirup-Jensen, S.; Carlström, A.; Hyltoft-Petersen, P.; Johnson, A. M.; Milford-Ward, A.; Ritchie, R. F.; Svendsen, P. J.; Whicker, J. Consensus of a Group of Professional Societies and Diagnostic Companies on Guidelines for Interim Reference Ranges for 14 Proteins in Serum Based on the Standardization against the IFCC/BCR/CAP Reference Material (CRM 470). *Clin. Chem. Lab. Med.* **1996**, *34*, 517−520.

(13) Constantine, N. T.; Zink, H. HIV Testing Technologies After Two Decades of Evolution. *Indian J. Med. Res.* **2005**, *121*, 519−538.

(14) Hu, W. P.; Lu, Y.; Precioso, N. A.; Chen, H. Y.; Howard, T.; Anderson, D.; Guan, M. Double-Antigen Enzyme-Linked Immunosorbent Assay for Detection of Hepatitis E Virus-Specific Antibodies in Human or Swine Sera. *Clin. Vaccine Immunol.* **2008**, *15*, 1151−1157.

(15) Fernandes, S. C.; Logounov, G. S.; Munro, J. B.; Mace, C. R. Comparison of Three Indirect Immunoassay Formats on a Common Paper-Based Microfluidic Device Architecture. *Anal. Methods* **2016**, *8*, 5204−5211.

(16) Liu, H.; Crooks, R. M. Three-Dimensional Paper Microfluidic Devices Assembled Using the Principles of Origami. *J. Am. Chem. Soc.* **2011**, *133*, 17564−17566.

(17) Carrilho, E.; Martinez, A. W.; Whitesides, G. M. Understanding Wax Printing: A Simple Micropatterning Process for Paper-Based Microfluidics. *Anal. Chem.* **2009**, *81*, 7091−7095.

(18) O'Farrell, B. Lateral Flow Immunoassay Systems: Evolution from the Current State of the Art to the Next Generation of Highly Sensitive, Quantitative Rapid Assays. In *The Immunoassay Handbook: Theory and Applications of Ligand Binding*; ELISA, 2013; pp 89−107.

(19) Miller, E. A.; Baniya, S.; Osorio, D.; Maalouf, Y. J. Al.; Sikes, H. D. Paper-Based Diagnostics in the Antigen-Depletion Regime: High-Density Immobilization of RcSso7d-Cellulose-Binding Domain Fusion Proteins for Efficient Target Capture. *Biosens. Bioelectron.* **2018**, *102*, 456−463.

(20) Leung, D. T. M.; Tam, F. C. H.; Ma, C. H.; Chan, P. K. S.; Cheung, J. L. K.; Niu, H.; Tam, J. S. L.; Lim, P. L. Antibody Response of Patients with Severe Acute Respiratory Syndrome (SARS) Targets the Viral Nucleocapsid. *J. Infect. Dis.* **2004**, *190*, 379−386.

(21) Shang, B.; Wang, X.-Y.; Yuan, J.-W.; Vabret, A.; Wu, X.-D.; Yang, R.-F.; Tian, L.; Ji, Y.-Y.; Deubel, V.; Sun, B. Characterization and Application of Monoclonal Antibodies against N Protein of SARS-Coronavirus. *Biochem. Biophys. Res. Commun.* **2005**, *336*, 110−117.

(22) Surjit, M.; Lal, S. K. The SARS-CoV Nucleocapsid Protein: A Protein with Multifarious Activities. *Infect. Genet. Evol.* **2008**, *8*, 397−405.

(23) Burbelo, P. D.; Riedo, F. X.; Morishima, C.; Rawlings, S.; Smith, D.; Das, S.; Strich, J. R.; Chertow, D. S.; Davey, R. T.; Cohen, J. I. Detection of Nucleocapsid Antibody to SARS-CoV-2 Is More Sensitive than Antibody to Spike Protein in COVID-19 Patients. *medRiv Preprint* **2020**, DOI: 10.1101/2020.04.20.20071423.

(24) Xu, X.; Sun, J.; Nie, S.; Li, H.; Kong, Y.; Liang, M.; Hou, J.; Huang, X.; Li, D.; Ma, T.; Peng, J.; Gao, S.; Shao, Y.; Zhu, H.; Lau, J. Y.-N.; Wang, G.; Xie, C.; Jiang, L.; Huang, A.; Yang, Z.; Zhang, K.; Hou, F. F. Seroprevalence of Immunoglobulin M and G Antibodies against SARS-CoV-2 in China. *Nat. Med.* **2020**, *26*, 1193−1195.

(25) http://www.diazyme.com/dz-lite-sars-cov-2 (Accessed on Sept 30, 2020).

(26) Patterson, E. I.; Prince, T.; Anderson, E. R.; Casas-Sanchez, A.; Smith, S. L.; Cansado-Utrilla, C.; Turtle, L.; Hughes, G. L. Methods of Inactivation of SARS-CoV-2 for Downstream Biological Assays. *bioRiv Preprint* **2020**, DOI: 10.1101/2020.05.21.108035.

(27) https://www.fda.gov/medical-devices/coronavirus-disease-2019-covid-19-emergency-use-authorizations-medical-devices/vitro-diagnostics-euas (Accessed on Sept 30, 2020).

(28) https://www.ncbi.nlm.nih.gov/protein/YP_009724397 (Accessed on Sept 30, 2020).

(29) Miller, E. A.; Traxlmayr, M. W.; Shen, J.; Sikes, H. D. Activity-Based Assessment of an Engineered Hyperthermophilic Protein as a Capture Agent in Paper-Based Diagnostic Tests. *Mol. Syst. Des. Eng.* **2016**, *1*, 377−381.

(30) Fairhead, M.; Howarth, M. Site-Specific Biotinylation of Purified Proteins Using BirA. *Methods Mol. Biol.* **2015**, *1266*, 171−184.

(31) Sung, K.-J.; Miller, E. A.; Sikes, H. D. Engineering Hyperthermostable RcSso7d as Reporter Molecule for in Vitro Diagnostic Tests. *Mol. Syst. Des. Eng.* **2018**, *3*, 877−882.

https://doi.org/10.1021/acssensors.1c00235
ACS Sens. XXXX, XXX, XXX−XXX